

UAV-enabled IoT Systems: NOMA or OMA?

Xidong Mu, *Student Member, IEEE*, Yuanwei Liu, *Senior Member, IEEE*,
 Li Guo, *Member, IEEE*, and Jiaru Lin, *Member, IEEE*

Abstract

This paper investigates unmanned aerial vehicle (UAV) enabled Internet-of-Things (IoT) systems with a couple of multiple access schemes, where a rotary-wing UAV is dispatched to collect data from multiple IoT devices. Our goal is to maximize the minimum UAV data collection throughput from IoT devices for both orthogonal multiple access (OMA) and non-orthogonal multiple access (NOMA) schemes, subject to the energy budgets of both the UAV and IoT devices. 1) For the OMA scheme, we propose an efficient algorithm by invoking alternating optimization (AO) method, where each subproblems are alternatively solved by applying successive convex approximation (SCA) technique. 2) For the NOMA scheme, we first handle subproblems with fixed decoding order with SCA technique. Then, we design a penalty-based algorithm to solve the decoding order design subproblem. Thus, we propose another AO-based algorithm to derive a locally optimal solution for the NOMA scheme. Numerical results illustrate that: 1) the proposed algorithms improve the max-min throughput performance compared with other benchmark schemes; 2) the NOMA scheme always achieves no worse performance than that of the OMA scheme.

I. INTRODUCTION

The Internet-of-Things (IoT) has received tremendous attention from both academia and industry in recent years. With a large number of physical objects connected to the Internet, there are a wide range of applications of the IoT technology, such as remote health care, traffic surveillance, public safety, etc [1–3]. During the applications, the low cost IoT devices can gather data from specific areas and send it back to the control station for further processing. However, the limited lifetime of IoT devices is one of critical issues since the equipped batteries of devices are usually not rechargeable [4]. On the other hand, massive connectivity is another requirement of IoT systems [5]. With the large amount number of devices, the networks need to support plenty of devices communication simultaneously, which brings new challenges to the IoT applications.

Recently, unmanned aerial vehicle (UAV) enabled IoT system has been considered as a

X. Mu, L. Guo, and J. Lin are with Beijing University of Posts and Telecommunications, Beijing, China (email:{muxidong, guoli, jrLin}@bupt.edu.cn).

Y. Liu is with Queen Mary University of London, London, UK (email:yuanwei.liu@qmul.ac.uk).

promising solution, where UAVs equipped with IoT sensing devices are deployed to collect data from IoT devices [6]. Compared with conventional IoT data collection system, IoT devices are able to upload data to UAVs directly through the line-of-sight (LoS) dominant UAV-ground channels [7], which leads to less energy consumption of devices. Besides, UAVs can also fly closer to those devices to enhance the quality of communication links. Therefore, the devices' lifetime are greatly prolonged in UAV-enabled IoT systems. On the other hand, thanks to the low cost and high flexibility features of UAVs, UAV-enabled IoT systems are more suitable for data collection from inaccessible regions, such as forest or marine monitoring, where deploying conventional terrestrial infrastructure to collect data is costly and inefficient. Additionally, non-orthogonal multiple access (NOMA) is identified as a critical technology for the next generation wireless networks owing to its superior performance in spectrum efficiency, massive connectivity and user fairness [8, 9]. Different from the conventional orthogonal multiple access (OMA), the key idea of power domain NOMA is allowing different users share the same time/frequency resource and multiplexed in power levels. At receivers, successive interference cancellation (SIC) technique is applied for extra interference cancelation and signal decoding. It has been proved that NOMA outperforms OMA in terms of the system sum rate based on the conventional communication system [10]. This motivate us to investigate the potential benefits of combining NOMA technology with UAV-enabled IoT systems.

A. Related Works

1) *Studies on NOMA Technology*: Significant efforts have been devoted to study NOMA technology in recent years. For example, Ding *et al.* [11] studied the downlink NOMA system with randomly deployed users, which shows NOMA outperforms OMA in terms of outage performance and sum rate performance. A power allocation scheme was proposed by Yang *et al.* [12] in both downlink and uplink NOMA scenarios while satisfying users' quality of service (QoS) requirements. Choi [13] designed the power allocation algorithm for downlink NOMA by taking user fairness into account. Furthermore, Liu *et al.* [14] investigated simultaneous wireless information and power transfer (SWIPT) technique with cooperative NOMA. In this model, stronger users improve the performance of weaker users by acting as relays with energy harvesting. Ali *et al.* [15] invoked coordinated multi-point (CoMP) transmission in multi-cell NOMA networks to improve the performance of cell-edge users. The secrecy performance of NOMA communication with artificial noise in large-scale networks was studied by Liu *et al.* [16]. Zhai *et al.* [17] proposed a dynamic user scheduling and power allocation scheme in downlink

NOMA-IoT networks, where stochastic optimization method was invoked to minimize the long-term energy consumption. Lv *et al.* [18] studied millimeter-wave NOMA-IoT communication systems, where the devices' outage probability and sum rate performance were analyzed with different pairing schemes. Wu *et al.* [19] compared the performance of TDMA and NOMA schemes in wireless powered IoT networks, which shows that TDMA scheme achieves higher spectral and energy efficiency since IoT devices in the NOMA scheme require more energy.

2) *Studies on UAV-enabled Communications:* UAV-enabled communications has drawn significant attentions of researchers in the past few years. In existing literatures, UAVs are deployed as aerial base stations (BSs), relays and users to boost the system performance such as coverage and capacity. In terms of UAVs' state in the sky, researches can be divided into two categories: static UAV and mobile UAV enabled communications. For the static UAV case, researchers mainly focused on the optimal deployment/placement of UAVs due to the unique air-to-ground (A2G) channel characteristics. Al-Hourani *et al.* [20] studied the optimal UAV altitude to maximize the coverage based on the probability A2G channel model. Mozaffari *et al.* [21] further investigated optimal three-dimensional (3D) deployment of multiple UAVs, where an efficient method was proposed to have maximum coverage while considering the inter-cell interference caused by different UAVs. Lyu *et al.* [22] proposed a spiral-based algorithm to use the minimum number of UAVs while ensuring all ground users are served. UAVs in coexistence with D2D communications were studied by Mozaffari *et al.* [23], where the user outage probability is analyzed in both static and mobile UAV scenarios. For the mobile UAV enabled communications, the mobility of UAVs were exploited to further improve the system performance, such as average throughput, secrecy rate, etc. A Multi-UAV BSs network was considered by Wu *et al.* [24], where the minimum average rate of ground users were maximized by optimizing UAVs' trajectories, transmit power and user scheduling. Secure transmission in UAV communications was studied by Cai *et al.* [25]. In this model, two UAVs are used for information transmission and jamming, respectively. The system secrecy rate was maximized by designing UAVs' trajectory and scheduling. You *et al.* [26] optimized 3D UAV trajectory in UAV-enabled data harvesting system with Rician fading channel model.

Despite the mentioned advantages of UAV-enabled communication, the limited UAV on-board energy is one of major challenges in practical UAV applications. To tackle this problem, a propulsion energy consumption model for rotary-wing UAVs were designed by Zeng *et al.* [27], where a novel path discretization method was proposed to minimize the UAV energy consumption.

Gong *et al.* [28] studied UAV flight time minimization problem in UAV data collection wireless sensor networks. Zhan *et al.* [29] minimized the energy consumption of IoT devices in a UAV-enabled IoT network while considering UAV energy constraints. Sun *et al.* [30] further studied solar-powered UAV communication systems, where the optimal UAV trajectory and resource allocation were designed with monotonic optimization.

3) *Studies on UAV-NOMA Systems:* Considering the advantages of UAV and NOMA technologies, some literatures has investigated UAV-NOMA systems [31]. For example, Sohail *et al.* [32] optimized the UAV attitude as well as power allocation to achieve maximum sum rate when UAV BSs serve ground users with NOMA. Hou *et al.* [33] investigated multiple antennas technique in UAV NOMA communications, where the system performance was analyzed with stochastic geometry approach in both LOS and NLoS scenarios. Mei *et al.* [34] proposed a novel uplink cooperative NOMA framework to tackle the UAV introduce interference. A resource allocation problem was formulated by Duan *et al.* [35] in uplink NOMA Multi-UAV IoT systems, where the system sum rate was maximized by optimizing subchannel allocation, IoT devices' transmit power and UAVs' attitude. Furthermore, Cui *et al.* [36] maximized the minimum achievable rate of GUEs by jointly optimizing the UAV trajectory, transmit power and user association in both downlink NOMA and OMA scenarios. A UAV-assisted NOMA network was proposed by Zhao *et al.* [37], where the UAV trajectory and precoding of the ground base station were jointly designed to maximize the system sum rate.

B. Motivation and Contributions

While the aforementioned research contributions have laid a solid foundation on NOMA and UAV systems, the investigations on the application of NOMA in UAV-enabled IoT systems are still quite open. As described before, the limited energy of UAVs and IoT devices need to be carefully considered while improving the system performance. To the best of our knowledge, there is the first work to investigate different multiple access schemes in the UAV-enabled IoT system. Dose NOMA still outperform OMA in such systems?

Driven by the above issue, in this article, we consider UAV-enabled IoT systems with different multiple access schemes. Specifically, the UAV flies from the predefined initial location to final location to harvest data from ground IoT devices under the UAV and IoT devices energy constraints. Our main contributions of this paper are summarized as follows:

- We propose energy limied UAV-enabled IoT by utilizing both OMA and NOMA schemes. By utilizing the proposed models, we formulate the minimum UAV data collection through-

put maximization problem by jointly optimizing the UAV trajectory, IoT devices' transmit power and scheduling, while taking the energy constraints of both UAV and IoT devices into consideration.

- For the OMA scheme, we develop an efficient algorithm with alternating optimization (AO) method, where each non-convex subproblems are solved by applying successive convex approximation (SCA) technique. We further prove that the proposed algorithm is convergent. We derive the performance upper bound by ignoring the UAV energy constraint.
- For the NOMA scheme, we propose a penalty-based algorithm for solving the mixed integer non-convex decoding order design subproblem, where the relaxed continuous variables are forced to be binaries through iterations. We demonstrate that the OMA scheme can be regarded as a special case of the NOMA scheme.
- Numerical results demonstrate that: 1) our designed algorithms for both schemes have a fast convergence speed; 2) the max-min throughput performance obtained by our proposed algorithm significantly outperforms other benchmark schemes; 3) the performance achieved by the NOMA scheme is always larger than or equal to that of the OMA scheme.

C. Organization and Notations

The rest of the paper is organized as follows. Section II presents the system model and problem formulations. In Section III and Section IV, two efficient AO-based algorithms for the OMA and NOMA scheme are developed. Section V provides the numerical results to validate the effectiveness of our proposed designs. Finally, Section VI concludes the paper.

Notations: Scalars are denoted by lower-case letters, vectors are denoted by bold-face lower-case letters. $\mathbb{R}^{M \times 1}$ denotes the space of M -dimensional real-valued vector. For a vector \mathbf{a} , \mathbf{a}^T denotes its transpose and $\|\mathbf{a}\|$ denotes its Euclidean norm.

II. SYSTEM MODEL AND PROBLEM FORMULATION

A. System Model

As shown in Fig.1, we consider a UAV-enabled IoT system, which consists of a rotary-wing UAV data collector and K IoT devices. The IoT devices are indexed by the set $\mathcal{K} = \{1, \dots, K\}$. The UAV is dispatched fly from the predefined initial location to the final location with a constant height H . During the flight, the UAV collects data from each IoT devices. Without loss of generality, a 3D Cartesian coordinate system is considered. The k th IoT device is fixed at $(\mathbf{w}_k^T, 0)^T$, where $\mathbf{w}_k = (x_k, y_k)^T$ denotes the corresponding horizontal coordinate. Similarly,

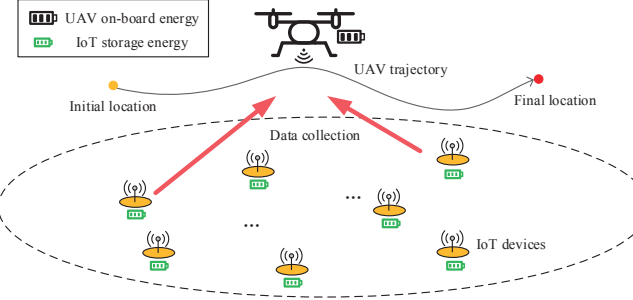


Fig. 1: Illustration of the UAV-enabled IoT system.

$(\mathbf{u}_I^T, H)^T$ and $(\mathbf{u}_F^T, H)^T$ are the UAV's predefined initial and final coordinates, where $\mathbf{u}_I = (x_I, y_I)^T$ and $\mathbf{u}_F = (x_F, y_F)^T$. Denote E_U and E_k as the UAV total on-board energy and the total storage energy of the k th IoT device, respectively. Let T_U denote the corresponding UAV total flight time, the instant UAV trajectory is defined as $(\mathbf{u}(t)^T, H)^T$, $0 \leq t \leq T_U$, where $\mathbf{u}(t) \in \mathbb{R}^{2 \times 1}$ is the UAV horizontal location. Different from the existing UAV trajectory design works with time discretization method [24–26], T_U is unknown and needs to be optimized in our work. To facilitate the designing of UAV trajectory, we invoke path discretization method [27] and divide the UAV path into N line segments with $N + 1$ waypoints, where $\mathbf{u}[1] = \mathbf{u}_I$, $\mathbf{u}[N + 1] = \mathbf{u}_F$. In order to achieve good approximation, we have following constraints:

$$\|\mathbf{u}[n + 1] - \mathbf{u}[n]\| \leq \delta, n = 1, \dots, N, \quad (1)$$

where δ is chosen sufficiently small compared with the UAV height such that the distance between the UAV and each devices is approximately unchanged and the UAV's speed is regard as a constant within each line segments. The time duration of n th line segment is denoted as $T[n]$ and $\sum_{n=1}^N T[n] = T_U$. The constraints introduced by the UAV mobility can be expressed as

$$\|\mathbf{u}[n + 1] - \mathbf{u}[n]\| \leq V_{\max} T[n], n = 1, \dots, N, \quad (2)$$

where V_{\max} denotes the maximum speed of the UAV.

According to recent air-to-ground (A2G) channel modeling literatures [20, 38], there is a high probability for A2G channel to be dominated by LoS link, especially for rural or suburban environment, which is also the typical scenario for UAV-enabled IoT systems. Therefore, the channel power gains between the UAV and the k th devices at the n th line segment can be expressed as

$$|h_k[n]|^2 = \frac{\rho_0}{\|\mathbf{u}[n] - \mathbf{w}_k\|^2 + H^2}, \quad (3)$$

where ρ_0 is the channel power gain at the reference distance of 1 meter.

In this paper, we adopt the propulsion power consumption model of rotary-wing UAVs in [27] which ignores the UAV acceleration energy consumption. Suppose that a rotary-wing UAV flying at the speed of V , the corresponding propulsion power consumption can be calculated as

$$P(V) = P_0 \left(1 + \frac{3V^2}{U_{tip}^2} \right) + P_i \left(\sqrt{1 + \frac{V^4}{4v_0^4}} - \frac{V^2}{2v_0^2} \right)^{1/2} + \frac{1}{2} d_0 \rho s A V^3, \quad (4)$$

where the first term and the third term represents blade profile power and parasite power, respectively. The second term represents the induced power. The relevant parameters are explained in [27]. During the n th line segment, the UAV speed can be calculated as $V[n] = \frac{s[n]}{T[n]}$, where $s[n] = \|\mathbf{u}[n+1] - \mathbf{u}[n]\|$. Thus, the UAV energy consumption at n th line segment is expressed as

$$\begin{aligned} E[n] &= T[n] P \left(\frac{s[n]}{T[n]} \right) \\ &= P_0 \left(T[n] + \frac{3s[n]^2}{U_{tip}^2 T[n]} \right) + P_i \left(\sqrt{T[n]^4 + \frac{s[n]^4}{4v_0^4}} - \frac{s[n]^2}{2v_0^2} \right)^{\frac{1}{2}} + \frac{1}{2} d_0 \rho s A \frac{s[n]^3}{T[n]^2}. \end{aligned} \quad (5)$$

Then, the total UAV energy constraint can be expressed as

$$\sum_{n=1}^N E[n] \leq E_U. \quad (6)$$

The sleep-wake protocol is considered for the UAV collects data from IoT devices. The devices upload information only when being waken up by the UAV, otherwise they keep in silence. Let $p_k[n]$ denote the transmit power of the k th IoT device at n th line segment. In the next subsection, we formulate the optimization problem with a couple of multiple access schemes, i.e., OMA and NOMA.

B. Problem Formulation for OMA Scheme

In the OMA data collection scheme, the UAV receives the information bits from different IoT devices by allocating unique time resources at each time duration $T[n]$. Let $\tau_k[n]$ denote the allocated time resources for the k th device during $T[n]$. We have the following constraints:

$$\sum_{k=1}^K \tau_k[n] \leq T[n], \forall n. \quad (7)$$

The achievable data collection throughput (bits/Hz) from the k th device during the n th line segment in the OMA scheme can be calculated as

$$r_k^O[n] = \tau_k[n] \log_2 \left(1 + \frac{\gamma_0 p_k[n]}{\|\mathbf{u}[n] - \mathbf{w}_k\|^2 + H^2} \right), \quad (8)$$

where $\gamma_0 = \frac{\rho_0}{\sigma^2}$. Therefore, the total achievable throughput from the k th device during the UAV flight is $Q_k^O = \sum_{n=1}^N r_k^O[n]$. In our work, the circuit power consumptions of IoT devices are ignored, the total storage energy constraint of the k th device in the OMA scheme can be expressed as:

$$\sum_{n=1}^N \tau_k[n] p_k[n] \leq E_k, \forall k. \quad (9)$$

In this paper, the UAV is assumed to have a priori known of the locations of all IoT devices, our objective is to maximize the minimum UAV data collection throughput from all IoT devices by jointly optimizing the UAV trajectory $\{\mathbf{u}[n], T[n]\}$, IoT device scheduling $\{\tau_k[n]\}$ and transmit power $\{p_k[n]\}$, while taking the energy constraints of both UAV and IoT devices into account. Then, the optimization problem can be formulated as

$$(P1) : \max_{\{\mathbf{u}[n], T[n], \tau_k[n], p_k[n]\}} \min_{\forall k} Q_k^O \quad (10a)$$

$$\text{s.t. } \mathbf{u}[1] = \mathbf{u}_I, \mathbf{u}[N] = \mathbf{u}_F, \quad (10b)$$

$$\|\mathbf{u}[n+1] - \mathbf{u}[n]\| \leq \min(\delta, V_{\max} T[n]), \forall n, \quad (10c)$$

$$\sum_{n=1}^N E[n] \leq E_U, \quad (10d)$$

$$\sum_{n=1}^N \tau_k[n] p_k[n] \leq E_k, \forall k, \quad (10e)$$

$$\sum_{k=1}^K \tau_k[n] \leq T[n], \forall n, \quad (10f)$$

$$\tau_k[n] \geq 0, \forall k, n, \quad (10g)$$

$$0 \leq p_k[n] \leq P_{\max}, \forall n, k, \quad (10h)$$

where P_{\max} represents the maximum transmit power of IoT devices. (10b) and (10c) represent the UAV mobility constraints. (6) and (10e) are energy constraints of the UAV and IoT devices, respectively.

Remark 1. For the OMA UAV data collection scheme in (P1), communication time resource allocation is performed in an adaptive manner. We refer to this type of OMA as OMA-II scheme. In traditional OMA communication systems, time resource is equally allocated to all IoT devices, which is defined as OMA-I scheme [10]. It is easy to transform Problem (P1) into OMA-I scheme with additional constraints, $\tau_k[n] = \tau_j[n], \forall k \neq j$.

C. Problem Formulation for NOMA Scheme

In uplink NOMA data collection scheme, the UAV receives all IoT devices' signals through the same time resource. Different from the downlink NOMA communication [36], where the SIC

decoding order is determined by the channel gains. In uplink NOMA, the UAV can perform SIC in any arbitrary order since all received signals at the UAV are desired signals. Let $\pi_n(k)$ denote the decoding order of IoT device k at the n th line segment. If $\pi_n(k) = i$, then device k is the i th signal to be decoded at n th line segment. Therefore, a set of binary indicators $\alpha_{k,m}[n] \in \{0, 1\}$ are defined as:

$$\alpha_{k,m}[n] = 1, \pi_n(k) > \pi_n(m), \quad (11)$$

$$\alpha_{k,m}[n] + \alpha_{m,k}[n] = 1. \quad (12)$$

Equation (12) ensures that there is only one device at each decoding orders. The UAV received signal-to-interference-plus-noise (SINR) of device k at the n th line segment can be expressed as

$$\begin{aligned} \gamma_k^N[n] &= \frac{\gamma_0 p_k[n] |h_k[n]|^2}{\sum_{m \in \mathcal{K}, m \neq k} \alpha_{m,k}[n] \gamma_0 p_m[n] |h_m[n]|^2 + 1} \\ &= \frac{\gamma_0 p_k[n] / (\|\mathbf{u}[n] - \mathbf{w}_k\|^2 + H^2)}{\sum_{m \in \mathcal{K}, m \neq k} \alpha_{m,k}[n] \gamma_0 p_m[n] / (\|\mathbf{u}[n] - \mathbf{w}_m\|^2 + H^2) + 1}. \end{aligned} \quad (13)$$

Let $\tau[n]$ denote the UAV allocated time resource for all IoT devices at n th line segment, where $\tau[n] \leq T[n], \forall n$. Similarly, the total achievable UAV data collection throughput from the k th device during the UAV flight in the NOMA scheme can be expressed as

$$Q_k^N[n] = \sum_{n=1}^N r_k^N[n] = \sum_{n=1}^N \tau[n] \log_2 (1 + \gamma_k^N[n]). \quad (14)$$

Meanwhile, we have the following IoT devices' energy constraints in the NOMA scheme:

$$\sum_{n=1}^N \tau[n] p_k[n] \leq E_k, \forall k. \quad (15)$$

By jointly optimizing the UAV trajectory $\{\mathbf{u}[n], T[n]\}$, communication time allocation $\{\tau[n]\}$, IoT devices transmit power $\{p_k[n]\}$ and decoding order $\{\alpha_{k,m}[n]\}$, the minimum data collection throughput maximization problem in the NOMA scheme can be formulated as

$$(P2) : \max_{\{\mathbf{u}[n], T[n], \tau[n], p_k[n], \alpha_{k,m}[n]\}} \min_{\forall k} Q_k^N \quad (16a)$$

$$\text{s.t. } \mathbf{u}[1] = \mathbf{u}_I, \mathbf{u}[N] = \mathbf{u}_F, \quad (16b)$$

$$\|\mathbf{u}[n+1] - \mathbf{u}[n]\| \leq \min(\delta, V_{\max} T[n]), \forall n, \quad (16c)$$

$$\sum_{n=1}^N E[n] \leq E_U, \quad (16d)$$

$$\sum_{n=1}^N \tau[n] p_k[n] \leq E_k, \forall k, \quad (16e)$$

$$0 \leq \tau[n] \leq T[n], \forall n, \quad (16f)$$

$$0 \leq p_k[n] \leq P_{\max}, \forall n, k, \quad (16g)$$

$$\alpha_{k,m}[n] + \alpha_{m,k}[n] = 1, \forall k \neq m \in \mathcal{K}, \quad (16h)$$

$$\alpha_{k,m}[n] \in \{0, 1\}, \forall k, m \in \mathcal{K}, \quad (16i)$$

Both Problem (P1) and (P2) are non-convex problem due to the non-convex objective function and constraints, where optimization variables are highly coupled. Moreover, Problem (P2) involves binary variables which make (P2) become a mixed integer non-convex problem. Therefore, it is difficult to solve find the global optimal solution for the two problems. In the following, we design efficient algorithms by utilizing AO method and SCA technique to find a high quality suboptimal solution for each problems.

III. PROPOSED SOLUTIONS FOR OMA SCHEME

To make Problem (P1) more tractable, we first introduce slack variables $\{\theta_k[n]\}$ and $\{\omega[n] \geq 0\}$ such that

$$\theta_k[n]^2 = \tau_k[n] B \log_2 \left(1 + \frac{\gamma_0 p_k[n]}{\|\mathbf{u}[n] - \mathbf{w}_k\|^2 + H^2} \right), \quad (17)$$

$$\omega[n] = \left(\sqrt{T[n]^4 + \frac{s[n]^4}{4v_0^4}} - \frac{s[n]^2}{2v_0^2} \right)^{\frac{1}{2}}, \forall n. \quad (18)$$

Moreover, equation (18) is equivalent to

$$\frac{T[n]^4}{\omega[n]^2} = \omega[n]^2 + \frac{s[n]^2}{v_0^2}. \quad (19)$$

With the above introduced variables and define $\eta^O = \min_{\forall k} Q_k^O$, we can obtain the following optimization problem

$$(P1.1) : \max_{\eta^O, \{\mathbf{u}[n], T[n], \tau_k[n], p_k[n], \theta_k[n], \omega[n]\}} \eta^O \quad (20a)$$

$$\text{s.t. } \sum_{n=1}^N \theta_k[n]^2 \geq \eta^O, \forall k, \quad (20b)$$

$$\frac{\theta_k[n]^2}{\tau_k[n]} \leq \log_2 \left(1 + \frac{\gamma_0 p_k[n]}{\|\mathbf{u}[n] - \mathbf{w}_k\|^2 + H^2} \right), \quad (20c)$$

$$P_0 \sum_{n=1}^N \left(T[n] + \frac{3s[n]^2}{U_{tip}^2 T[n]} \right) + P_i \sum_{n=1}^N \omega[n] \quad (20d)$$

$$+ \frac{1}{2} d_0 \rho s A \sum_{n=1}^N \frac{s[n]^3}{t[n]^2} \leq E_U,$$

$$\frac{T[n]^4}{\omega[n]^2} \leq \omega[n]^2 + \frac{\|\mathbf{u}[n+1] - \mathbf{u}[n]\|^2}{v_0^2}, \forall n, \quad (20e)$$

$$(10b), (10c), (10e) - (10h). \quad (20f)$$

Proposition 1. Problem (P1.1) is equivalent to Problem (P1).

Proof. Without loss of optimality to Problem (P1.1), constraints (20c) and (20e) can be met with equality. Specifically, assume that if any of the constraint in (20c) is satisfied with strict inequality, then we can always increase $\theta_k[n]^2$ to make the constraint (20c) satisfied with equality without decreasing the objective value. Furthermore, suppose that (20e) are satisfied with strict inequality, we can always reduce $\omega[n]$ to make the constraint (20e) satisfied with equality with other variables fixed, and at the same time make the constraint (20d) still satisfied without changing the objective value of (P1.1). Therefore, Problem (P1.1) is equivalent to Problem (P1). \square

Based on Proposition 1, we only need to focus on how to solve Problem (P1.1). Recall the fact that perspective operation preserves convexity [39], the first and third terms in (20d) are all convex functions jointly with respect to $s[n]$ and $T[n]$. As a result, (20d) is a convex constraint. In order to tackle the highly coupled non-convex constraints, we decompose the original problem (P1.1) into two subproblems in the following subsections.

A. Optimization with Fixed Transmit Power

Under any given feasible transmit power $\{p_k[n]\}$, the optimization problem can be written as

$$(P1.2) : \max_{\eta^O, \{\mathbf{u}[n], T[n], \tau_k[n], \theta_k[n], \omega[n]\}} \eta^O \quad (21a)$$

$$\text{s.t. } (10b), (10c), (10e) - (10f), (20b) - (20e). \quad (21b)$$

Problem (P1.2) is still a non-convex problem due to the non-convex constraints (20b), (20c) and (20e). Fortunately, those non-convex constraints can be handled by utilizing SCA technique with their lower bounds at given local points. Specifically, to tackle the non-convex constraint (20b), the left hand side (LHS) is a convex function with respect to $\theta_k[n]$. Since any convex functions are lower bounded by their first-order Taylor expansion, the lower bound of $\theta_k[n]^2$ at given local points $\theta_k^l[n]$ can be expressed as

$$\theta_k[n]^2 \geq \theta_k^l[n]^2 + 2\theta_k^l[n](\theta_k[n] - \theta_k^l[n]). \quad (22)$$

For the non-convex constraint (20c), the LHS is jointly convex with respect to $\theta_k[n]$ and $\tau_k[n]$. Though the right hand side (RHS) is not concave with respect to $\mathbf{u}[n]$, it is a convex function with respect to $\|\mathbf{u}[n] - \mathbf{w}_k\|^2$. With given local points $\{\mathbf{u}^l[n]\}$, the lower bound for the RHS of (20c) can be obtained as

$$\begin{aligned} \log_2 \left(1 + \frac{\gamma_0 p_k^l[n]}{\|\mathbf{u}[n] - \mathbf{w}_k\|^2 + H^2} \right) &\geq R_k^{low}[n] \\ &= \log_2 \left(1 + \frac{\gamma_0 p_k[n]}{\|\mathbf{u}^l[n] - \mathbf{w}_k\|^2 + H^2} \right) - \varphi_k^l[n] \left(\|\mathbf{u}[n] - \mathbf{w}_k\|^2 - \|\mathbf{u}^l[n] - \mathbf{w}_k\|^2 \right), \end{aligned} \quad (23)$$

where $\varphi_k^l[n] = \frac{(\log_2 e) \gamma_0 p_k[n]}{(\|\mathbf{u}^l[n] - \mathbf{w}_k\|^2 + H^2)(\|\mathbf{u}^l[n] - \mathbf{w}_k\|^2 + H^2 + \gamma_0 p_k[n])}$.

Similarly, to deal with the non-convex constraint (20e), the RHS is the sum of two convex functions and the lower bound is given by

$$\omega[n]^2 + \frac{\|\mathbf{u}[n+1] - \mathbf{u}[n]\|^2}{v_0^2} \geq \beta^{low}[n], \quad (24)$$

where

$$\begin{aligned} \beta^{low}[n] &= \omega^l[n]^2 + \omega^l[n] (\omega[n] - \omega^l[n]) - \frac{\|\mathbf{u}^l[n+1] - \mathbf{u}^l[n]\|^2}{v_0^2} \\ &\quad + \frac{2}{v_0^2} (\mathbf{u}^l[n+1] - \mathbf{u}^l[n])^T (\mathbf{u}[n+1] - \mathbf{u}[n]). \end{aligned}$$

By applying (22)-(24), Problem (P1.2) is approximate as the following optimization problem:

$$(P1.3) : \max_{\eta^O, \{\mathbf{u}[n], T[n], \tau_k[n], \theta_k[n], \omega[n]\}} \eta^O \quad (25a)$$

$$\text{s.t. } \sum_{n=1}^N (\theta_k^l[n]^2 + 2\theta_k^l[n] (\theta_k[n] - \theta_k^l[n])) \geq \eta^O, \forall k, \quad (25b)$$

$$\frac{\theta_k[n]^2}{\tau_k[n]} \leq R_k^{low}[n], \forall k, n, \quad (25c)$$

$$\frac{T[n]^4}{\omega[n]^2} \leq \beta^{low}[n], \forall n, \quad (25d)$$

$$(10b), (10c), (10e) - (10f), (20d). \quad (25e)$$

Now, it can be verified that Problem (P1.3) is a convex problem, which can be efficiently solved by standard convex optimization solvers such as CVX [40]. It is worth noting that the adoption of lower bounds in (22)-(24) results in the feasible region of (P1.3) is a subset of that of (P1.2). Thus, the optimal objective value of Problem (P1.3) in general provides a lower bound to that of Problem (P1.2).

B. Optimization with Fixed UAV Locations

Before solving this subproblem, we introduce another slack variables $\{\varepsilon_k[n]\}$ such that

$$\varepsilon_k[n]^2 = \tau_k[n] p_k[n], \forall n, k. \quad (26)$$

Thus, constraint (10e) can be equivalently expressed by the following two constraints:

$$\sum_{n=1}^N \varepsilon_k[n]^2 \leq E_k, \forall k, \quad (27)$$

$$p_k[n] \leq \frac{\varepsilon_k[n]^2}{\tau_k[n]}, \forall n, k. \quad (28)$$

Given any feasible UAV location $\{\mathbf{u}[n]\}$, Problem (P1.1) can be written as the following optimization problem:

$$(P1.4) : \max_{\eta^O, \{T[n], \tau_k[n], p_k[n], \theta_k[n], \omega[n], \varepsilon_k[n]\}} \eta^O \quad (29a)$$

$$\text{s.t. } (10f) - (10h), (20b) - (20e), (27), (28). \quad (29b)$$

Now, constraint (20c) is convex since the RHS is a concave function with respect to $p_k[n]$. However, Problem (P1.4) is still a non-convex problem due to the non-convex constraints (20b), (20e) and (28). As described before, we have introduced how to deal with non-convex constraints (20b) and (20e) with their lower bounds by applying the first-order Taylor expansion. Therefore, we only need to concentrate on how to deal with the non-convex constraint (28). Similarly, the RHS of (28) is jointly convex with respect to $\varepsilon_k[n]$ and $\tau_k[n]$. The lower bound with given local points $\{\varepsilon_k^l[n], \tau_k^l[n]\}$ can be expressed as

$$\begin{aligned} \frac{\varepsilon_k[n]^2}{\tau_k[n]} &\geq \frac{\varepsilon_k^l[n]^2}{\tau_k^l[n]} + \frac{2\varepsilon_k^l[n]}{\tau_k^l[n]} (\varepsilon_k[n] - \varepsilon_k^l[n]) \\ &\quad - \frac{\varepsilon_k^l[n]^2}{\tau_k^l[n]^2} (\tau_k[n] - \tau_k^l[n]), \forall n, k, \end{aligned} \quad (30)$$

By replacing the non-convex constraints with their lower bounds, Problem (P1.4) can be written as the following approximate optimization problem:

$$(P1.5) : \max_{\eta^O, \{T[n], \tau_k[n], p_k[n], \theta_k[n], \omega[n], \varepsilon_k[n]\}} \eta^O \quad (31a)$$

$$\text{s.t. } \sum_{n=1}^N (\theta_k^l[n]^2 + 2\theta_k^l[n] (\theta_k[n] - \theta_k^l[n])) \geq \eta^O, \forall k, \quad (31b)$$

$$\begin{aligned} p_k[n] &\leq \frac{\varepsilon_k^l[n]^2}{\tau_k^l[n]} + \frac{2\varepsilon_k^l[n]}{\tau_k^l[n]} (\varepsilon_k[n] - \varepsilon_k^l[n]) \\ &\quad - \frac{\varepsilon_k^l[n]^2}{\tau_k^l[n]^2} (\tau_k[n] - \tau_k^l[n]), \forall n, k, \end{aligned} \quad (31c)$$

$$\frac{T[n]^4}{\omega[n]^2} \leq \omega^l[n]^2 + 2\omega^l[n] (\omega[n] - \omega^l[n]) + \frac{s[n]^2}{v_0^2}, \forall n, \quad (31d)$$

$$(10f) - (10h), (20c), (20d), (27). \quad (31e)$$

It can be verified that Problem (P1.5) is a convex problem, which can be efficiently solved by standard convex optimization solvers such as CVX [40]. Similarly, the optimal objective value obtained from Problem (P1.5) serves a lower bound of that of Problem (P1.4) owing to the

replacement of non-convex terms with their lower bounds.

C. Overall Algorithm, Complexity and Convergence

Based on the two subproblems in the previous subsections, we propose an efficient algorithm to solve Problem (P1.1) by invoking AO method. Specifically, Problem (P1.3) and (P1.5) are alternatively solved. The obtained solutions in each iteration are used as the input local points for the next iteration. The details of the proposed algorithm for the OMA scheme are summarized in **Algorithm 1**. The complexity of each subproblems with interior-point method are $\mathcal{O}((3N + 2NK)^{3.5})$ and $\mathcal{O}((2N + 4NK)^{3.5})$. Then, the total complexity for the OMA scheme is $\mathcal{O}(N_{ite}^O((5N + 6NK)^{3.5}))$, where N_{ite}^O is the iteration number of Algorithm 1.

Algorithm 1 AO-based Algorithm for Problem (P1.1)

Initialize feasible solutions $\{\mathbf{u}^0[n], T^0[n], \tau_k^0[n], p_k^0[n]\}$ to (P1.1), $l = 0$.

- 1: **repeat**
- 2: Solve Problem (P1.3) for given $\{p_k^l[n]\}$, and denote the optimal solutions as $\{\mathbf{u}^{l+1}[n], T^{l+0.5}[n], \tau_k^{l+0.5}[n]\}$.
- 3: Solve Problem (P1.5) for given $\{\mathbf{u}^{l+1}[n]\}$, and denote the optimal solutions as $\{p_k^{l+1}[n], T^{l+1}[n], \tau_k^{l+1}[n]\}$.
- 4: $l = l + 1$.
- 5: **until** the fractional decrease of the objective value is below a threshold $\xi > 0$.

Remark 2. While Algorithm 1 is designed for OMA-II UAV-enabled IoT data collection scheme, it can be also applied for OMA-I scheme with additional linear constraints: $\tau_k[n] = \tau_j[n], \forall k \neq j$.

Next, we demonstrate the convergence of Algorithm 1. The objective value of Problem (P1.1) in the l th iteration is defined as $\eta^O(\{\mathbf{u}^l[n]\}, \{T^l[n]\}, \{\tau_k^l[n]\}, \{p_k^l[n]\})$. First, for Problem (P1.3) with given transmit power in step 2 of Algorithm 1, we have

$$\begin{aligned}
 & \eta^O(\{\mathbf{u}^l[n]\}, \{T^l[n]\}, \{\tau_k^l[n]\}, \{p_k^l[n]\}) \\
 & \stackrel{(a)}{=} \eta_{\mathbf{u}}^{lb}(\{\mathbf{u}^l[n]\}, \{T^l[n]\}, \{\tau_k^l[n]\}, \{p_k^l[n]\}) \\
 & \stackrel{(b)}{\leq} \eta_{\mathbf{u}}^{lb}(\{\mathbf{u}^{l+1}[n]\}, \{T^{l+0.5}[n]\}, \{\tau_k^{l+0.5}[n]\}, \{p_k^l[n]\}) \\
 & \stackrel{(c)}{\leq} \eta^O(\{\mathbf{u}^{l+1}[n]\}, \{T^{l+0.5}[n]\}, \{\tau_k^{l+0.5}[n]\}, \{p_k^l[n]\}),
 \end{aligned} \tag{32}$$

where $\eta_{\mathbf{u}}^{lb}$ represents the objective value of Problem (P1.3). (a) follows the fact that the first-order Taylor expansions are tight at the given local points in Problem (P1.3); (b) holds since Problem (P1.3) is solved optimally; (c) holds due to the fact that the objective value of Problem (P1.3)

serves the lower bound of that of (P1.2). It suggests that the objective value of Problem (P1.2) is non-decreasing after solving Problem (P1.3).

Similarly, for Problem (P1.5) with given UAV locations in step 3 of Algorithm 1, we have

$$\begin{aligned}
& \eta^O(\{\mathbf{u}^{l+1}[n]\}, \{T^{l+0.5}[n]\}, \{t_k^{l+0.5}[n]\}, \{p_k^l[n]\}) \\
&= \eta_p^{lb}(\{\mathbf{u}^{l+1}[n]\}, \{T^{l+0.5}[n]\}, \{t_k^{l+0.5}[n]\}, \{p_k^l[n]\}) \\
&\leq \eta_p^{lb}(\{\mathbf{u}^{l+1}[n]\}, \{T^{l+1}[n]\}, \{t_k^{l+1}[n]\}, \{p_k^{l+1}[n]\}) \\
&\leq \eta^O(\{\mathbf{u}^{l+1}[n]\}, \{T^{l+1}[n]\}, \{t_k^{l+1}[n]\}, \{p_k^{l+1}[n]\}),
\end{aligned} \tag{33}$$

where η_p^{lb} represents the objective value of Problem (P1.5).

As a result, based on (32) and (33), we obtain that

$$\begin{aligned}
& \eta^O(\{\mathbf{u}^l[n]\}, \{T^l[n]\}, \{t_k^l[n]\}, \{p_k^l[n]\}) \\
&\leq \eta^O(\{\mathbf{u}^{l+1}[n]\}, \{T^{l+1}[n]\}, \{t_k^{l+1}[n]\}, \{p_k^{l+1}[n]\}).
\end{aligned} \tag{34}$$

(34) means the objective value of Problem (P1.1) is non-decreasing after each iteration. Since the minimum UAV data collection throughput is upper bounded by a finite value, the proposed algorithm is guaranteed to converge to a locally optimal solution of Problem (P1.1).

D. Optimal Solution to (P1) without UAV Energy Constraint

In this subsection, we consider Problem (P1) without the UAV energy constraint. In this case, the optimal result is achieved by making the UAV hover on the top of each IoT devices for data collection, since otherwise the UAV can always fly closer to the IoT devices and achieve higher throughput. Let t_k denote the total data collection time when the UAV hovers on the top of device k and p_k is the transmit power of device k . The optimization problem can be written as

$$(P3) : \max_{\eta^\infty, \{t_k, p_k\}} \eta^\infty \tag{35a}$$

$$\text{s.t. } t_k \log_2 (1 + \gamma_h p_k) \geq \eta^\infty, \forall k, \tag{35b}$$

$$t_k p_k \leq E_k, \forall k, \tag{35c}$$

$$t_k \geq 0, 0 \leq p_k \leq p_{\max}, \forall k, \tag{35d}$$

where $\gamma_h = \frac{\gamma_0}{H^2}$. It can be verified that without loss of optimality to problem (P3), all constraints (35c) can be met with equality, since otherwise we can always increase t_k or p_k without decreasing the objective value. Thus, Problem (P3) can be equivalently expressed as

$$(P3.1) : \max_{\eta^\infty, \{t_k\}} \eta^\infty \tag{36a}$$

$$\text{s.t. } t_k \log_2 \left(1 + \frac{E_k \gamma_h}{t_k} \right) \geq \eta^\infty, \forall k, \tag{36b}$$

$$t_k \geq 0, \forall k. \quad (36c)$$

Problem (P3.1) can be decomposed into K independent subproblems. For example, the k th subproblem is expressed as

$$(P3.2) : \max_{t_k} f(t_k) \quad (37a)$$

$$\text{s.t. } t_k \geq 0, \quad (37b)$$

where $f(t_k) = t_k \log_2 \left(1 + \frac{E_k \gamma_h}{t_k}\right)$. Then, we have the following lemma to solve Problem (P3.2):

Lemma 1. $f(t_k)$ is an increasing function with respect to t_k . The optimal objective value of Problem (P3.2) is $\frac{E_k \gamma_h}{\ln 2}$.

Proof. Since the second order derivation of $f(t_k)$ is $f''(t_k) = -\frac{E_k^2 \gamma_h^2}{t_k (t_k + E_k \gamma_h) \ln 2} < 0$, which indicates the first order derivation $f'(t_k) = \log_2 \left(1 + \frac{E_k \gamma_h}{t_k}\right) - \frac{E_k \gamma_h}{t_k + E_k \gamma_h}$ is a decreasing function. Furthermore, since $f'(t_k) > f'(+\infty) = 0$, $f(t_k)$ is a increasing function. The maximum value is $\lim_{t_k \rightarrow +\infty} f(t_k) = \frac{E_k \gamma_h}{\ln 2}$. The proof is completed. \square

Based **Lemma 1**, K subproblems can be efficiently solved and the optimal result of Problem (P3) is $\eta^\infty = \min \left\{ \frac{E_k \gamma_h}{\ln 2}, \forall k \right\}$.

Remark 3. It is worth pointing out that since the UAV always has a finite value on-board energy, the maximum objective value of Problem (P1) is strictly upper bounded by the optimal result of (P3) obtained by Lemma 1.

IV. PROPOSED SOLUTIONS FOR NOMA SCHEME

In the NOMA scheme, we can use the same method to tackle the non-convex UAV energy constraint as described in the former section. Besides $\{\omega[n] \geq 0\}$, we introduce auxiliary variables $\{S_k[n]\}$, $\{I_k[n]\}$, $\{d_k[n]\}$ and $\{\theta_k[n]\}$ such that

$$S_k[n] = \frac{\|\mathbf{u}[n] - \mathbf{w}_k\|^2 + H^2}{\gamma_0 p_k[n]}, \forall k, n, \quad (38)$$

$$I_k[n] = \sum_{m \in \mathcal{K}, m \neq k} \gamma_0 \alpha_{m,k}[n] p_m[n] d_m[n]^{-1} + 1, \forall k, n, \quad (39)$$

$$d_k[n] = \|\mathbf{u}[n] - \mathbf{w}_k\|^2 + H^2, \forall k, n, \quad (40)$$

$$\theta_k[n]^2 = \tau[n] B \log_2 \left(1 + \frac{1}{S_k[n] I_k[n]}\right), \forall k, n. \quad (41)$$

Similarly, Problem (P2) can be equivalently rewritten as

$$(P2.1) : \max_{\eta^N, \left\{ \begin{array}{l} \mathbf{u}[n], T[n], \tau[n], p_k[n], \alpha_{k,m}[n] \\ S_k[n], I_k[n], \theta_k[n], \omega[n], d_k[n] \end{array} \right\}} \eta^N \quad (42a)$$

$$\text{s.t. } \sum_{n=1}^N \theta_k[n]^2 \geq \eta^N, \forall k, \quad (42b)$$

$$\frac{\theta_k[n]^2}{\tau[n]} \leq \log_2 \left(1 + \frac{1}{S_k[n] I_k[n]} \right), \forall k, n, \quad (42c)$$

$$S_k[n] \geq \frac{\|\mathbf{u}[n] - \mathbf{w}_k\|^2 + H^2}{\gamma_0 p_k[n]}, \forall k, n, \quad (42d)$$

$$I_k[n] \geq \sum_{m \in \mathcal{K}, m \neq k} \gamma_0 \alpha_{m,k}[n] p_m[n] d_m[n]^{-1} + 1, \forall k, n, \quad (42e)$$

$$d_k[n] \leq \|\mathbf{u}[n] - \mathbf{w}_k\|^2 + H^2, \forall k, n, \quad (42f)$$

$$P_0 \sum_{n=1}^N \left(T[n] + \frac{3s[n]^2}{U_{tip}^2 T[n]} \right) + P_i \sum_{n=1}^N \omega[n] + \frac{1}{2} d_0 \rho s A \sum_{n=1}^N \frac{s[n]^3}{t[n]^2} \leq E_U, \quad (42g)$$

$$\frac{T[n]^4}{\omega[n]^2} \leq \omega[n]^2 + \frac{\|\mathbf{u}[n+1] - \mathbf{u}[n]\|^2}{v_0^2}, \forall n, \quad (42h)$$

$$(16b), (16c), (16e) - (16i). \quad (42i)$$

The equivalence between (P2) and (P2.1) can be similarly proved as Theorem 1. It is observed that Problem (P2.1) has a similar structure as Problem (P1.1) except the integer constraint. Therefore, we still decompose (P2.1) into several subproblems, which are easier to handle.

A. Optimization with Fixed Transmit Power and Decoding Order

Given any feasible transmit power $\{p_k[n]\}$ and decoding order $\{a_{k,m}[n]\}$, the optimization problem can be written as

$$(P2.2) : \max_{\eta^N, \{\mathbf{u}[n], T[n], \tau[n], S_k[n]\}} \eta^N \quad (43a)$$

$$\text{s.t. } (16b), (16c), (16e), (16f), (42b) - (42h). \quad (43b)$$

Problem (P2.2) is still non-convex owing to the non-convex constraints (42b), (42c), (42f) and (42h). Specifically, (42b) and (42h) can be handled with the same manner as introduced in the previous section. Before handling the non-convex constraint (42c), we first have the following lemma:

Lemma 2. For $x > 0$ and $y > 0$, $f(x, y) = \log_2 \left(1 + \frac{1}{xy} \right)$ is a convex function with respect to x and y .

Proof. It is easy to prove lemma 2 by showing the Hessian matrix of function $f(x, y)$ is positive semidefinite when $x > 0$ and $y > 0$. As a result, $f(x, y)$ is a convex function. \square

Based on Lemma 2, the RHS of (42c) is jointly convex with respect to $S_k[n]$ and $I_k[n]$. Thus, by applying the first-order Taylor explanation, the lower bound at given local points $\{S_k^l[n], I_k^l[n]\}$ can be expressed as

$$\begin{aligned} \log_2 \left(1 + \frac{1}{S_k[n] I_k[n]} \right) &\geq R_k^{low}[n] = \log_2 \left(1 + \frac{1}{S_k^l[n] I_k^l[n]} \right) \\ &- \frac{(\log_2 e) (S_k[n] - S_k^l[n])}{S_k^l[n] + S_k^l[n]^2 I_k^l[n]} - \frac{(\log_2 e) (I_k[n] - I_k^l[n])}{I_k^l[n] + I_k^l[n]^2 S_k^l[n]}. \end{aligned} \quad (44)$$

Furthermore, for the non-convex constraints (42f), the RHS is a convex function with respect to $\mathbf{u}[n]$. The corresponding lower bound at given local points $\mathbf{u}^l[n]$ is expressed as

$$\|\mathbf{u}[n] - \mathbf{w}_k\|^2 \geq \|\mathbf{u}^l[n] - \mathbf{w}_k\|^2 + 2(\mathbf{u}^l[n] - \mathbf{w}_k)^T (\mathbf{u}[n] - \mathbf{u}^l[n]). \quad (45)$$

Therefore, Problem (P2.2) is approximated as the following optimization problem:

$$(P2.3) : \max_{\eta^N, \left\{ \begin{array}{l} \mathbf{u}[n], T[n], \tau[n], S_k[n] \\ I_k[n], \theta_k[n], \omega[n], d_k[n] \end{array} \right\}} \eta^N \quad (46a)$$

$$\text{s.t. } \sum_{n=1}^N (\theta_k^l[n]^2 + 2\theta_k^l[n](\theta_k[n] - \theta_k^l[n])) \geq \eta^N, \forall k, \quad (46b)$$

$$\frac{\theta_k[n]^2}{\tau_k[n]} \leq R_k^{low}[n], \forall k, n, \quad (46c)$$

$$d_k[n] \leq H^2 + \|\mathbf{u}^l[n] - \mathbf{w}_k\|^2 + 2(\mathbf{u}^l[n] - \mathbf{w}_k)^T (\mathbf{u}[n] - \mathbf{u}^l[n]), \quad (46d)$$

$$\frac{T[n]^4}{\omega[n]^2} \leq \beta^{low}[n], \forall n, \quad (46e)$$

$$(16b), (16c), (16e), (16f), (42d), (42e), (42g). \quad (46f)$$

Problem (P2.3) is a convex problem that can be efficiently solved by standard convex optimization solvers such as CVX [40]. Similarly, the optimal objective value obtained from Problem (P2.3) provides a lower bound to that of Problem (P2.2).

B. Optimization with Fixed UAV Locations and Decoding Order

Given any feasible UAV location $\{\mathbf{u}[n]\}$ and decoding order $\{a_{k,m}[n]\}$, Problem (P2.1) with auxiliary variables $\{\varepsilon[n]\}$ can be written as the following optimization problem:

$$(P2.4) : \max_{\eta^N, \left\{ \begin{array}{l} T[n], \tau[n], p_k[n], S_k[n] \\ I_k[n], \theta_k[n], \omega[n], \varepsilon[n], d_k[n] \end{array} \right\}} \eta^N \quad (47a)$$

$$\text{s.t. } \sum_{n=1}^N \varepsilon_k[n]^2 \leq E_k, \forall k, \quad (47b)$$

$$p_k[n] \leq \frac{\varepsilon_k[n]^2}{\tau[n]}, \forall n, k, \quad (47c)$$

$$(16f), (16g), (42b) - (42h). \quad (47d)$$

By replacing those non-convex terms involved in Problem (P2.4) with their lower bounds, (P2.4) is approximated as the following problem:

$$(P2.5) : \max_{\eta^N, \{T[n], \tau[n], p_k[n], S_k[n] \}_{I_k[n], \theta_k[n], \omega[n], \varepsilon[n], d_k[n]}} \eta^N \quad (48a)$$

$$\text{s.t. } \sum_{n=1}^N (\theta_k^l[n]^2 + 2\theta_k^l[n](\theta_k[n] - \theta_k^l[n])) \geq \eta^N, \forall k, \quad (48b)$$

$$\frac{\theta_k[n]^2}{\tau[n]} \leq R_k^{low}[n], \forall k, n, \quad (48c)$$

$$\begin{aligned} p_k[n] &\leq \frac{\varepsilon_k^l[n]^2}{\tau^l[n]} + \frac{2\varepsilon_k^l[n]}{\tau^l[n]} (\varepsilon_k[n] - \varepsilon_k^l[n]) \\ &\quad - \frac{\varepsilon_k^l[n]^2}{\tau^l[n]^2} (\tau[n] - \tau^l[n]), \forall n, k, \end{aligned} \quad (48d)$$

$$\frac{T[n]^4}{\omega[n]^2} \leq \omega^l[n]^2 + 2\omega^l[n](\omega[n] - \omega^l[n]) + \frac{s[n]^2}{v_0^2}, \forall n, \quad (48e)$$

$$(16f), (16g), (42d) - (42g). \quad (48f)$$

Currently, Problem (P2.5) is a convex problem that can be efficiently solved by standard convex optimization solvers such as CVX [40]. The optimal objective value obtained from Problem (P2.5) serves a lower bound of that of Problem (P2.4).

C. Decoding Order Design with Other Variables Fixed

Given any feasible UAV trajectory $\{\mathbf{u}[n], T[n]\}$, time allocation $\{\tau[n]\}$ and device transmit power $\{p_k[n]\}$, the optimization problem (P2.1) is reduced to

$$(P2.6) : \max_{\eta^N, \{a_{k,m}[n], I_k[n]\}} \eta^N \quad (49a)$$

$$\text{s.t. } \sum_{n=1}^N \tau[n] \log_2 \left(1 + \frac{1}{S_k[n] I_k[n]} \right) \geq \eta^N, \forall k, \quad (49b)$$

$$(16h), (16i), (42e). \quad (49c)$$

Involving the integer constraint (16i) and non-convex constraint (49b), Problem (P2.6) is mixed-integer non-convex problem. The integer constraint (16i) can be equivalently transformed into the following two constraints:

$$\sum_{k=1}^K \sum_{m \neq k}^K (\alpha_{k,m}[n]^2 - \alpha_{k,m}[n]) \geq 0, \quad (50)$$

$$0 \leq \alpha_{k,m}[n] \leq 1, \forall k \neq m \in \mathcal{K}. \quad (51)$$

Consequently, Problem (P2.6) can be reformulated with continuous variables $\{\alpha_{k,m}[n]\}$ as follow:

$$(P2.7) : \max_{\eta^N, \{\alpha_{k,m}[n], I_k[n]\}} \eta^N \quad (52a)$$

$$\text{s.t. (16h), (42e), (49b), (50), (51).} \quad (52b)$$

Though removing the integer constraint, Problem (P2.7) is still a non-convex problem with the non-convex constraints (49b) and (50). Before handling Problem (P2.7), we first have the following theorem:

Theorem 1. For a sufficiently large constant value $\lambda \gg 1$, Problem (P2.7) is equivalent to the following problem:

$$(P2.8) : \max_{\eta^N, \{\alpha_{k,m}[n], I_k[n]\}} \eta^N + \lambda \sum_{k=1}^K \sum_{m \neq k}^K (\alpha_{k,m}[n]^2 - \alpha_{k,m}[n]) \quad (53a)$$

$$\text{s.t. (16h), (42e), (49b), (51).} \quad (53b)$$

where λ represents a penalty factor to penalize the objective function for any $\alpha_{k,m}[n]$ that is not equal to 0 or 1.

Proof. See Appendix A. \square

To handle Problem (P2.8), we only need to deal with the non-convex objective function (53a) and non-convex constraints (49b). The second term of (53a) is a convex function with respect to $\alpha_{k,m}[n]$. By utilizing the first-order Taylor expansion at given local points $\alpha_{k,m}^l[n]$, the lower bound is expressed as

$$\alpha_{k,m}[n]^2 \geq \xi_{k,m}[n] = \alpha_{k,m}^l[n]^2 + 2\alpha_{k,m}^l[n](\alpha_{k,m}[n] - \alpha_{k,m}^l[n]). \quad (54)$$

For the non-convex constraint (49b), the LHS is a convex function with respect to $I_k[n]$. Similarly, the lower bound at given local points $\{I_k^l[n]\}$ is expressed as

$$\log_2 \left(1 + \frac{1}{S_k[n] I_k[n]} \right) \geq \log_2 \left(1 + \frac{1}{S_k[n] I_k^l[n]} \right) - \frac{(\log_2 e)(I_k[n] - I_k^l[n])}{I_k^l[n] + S_k[n] I_k^l[n]^2}. \quad (55)$$

Based on (54) and (55), Problem (P2.8) can be approximately written as

$$(P2.9) : \max_{\eta^N, \{\alpha_{k,m}[n], I_k[n]\}} \eta^N + \lambda \sum_{k=1}^K \sum_{m \neq k}^K (\xi_{k,m}[n] - \alpha_{k,m}[n]) \quad (56a)$$

$$\text{s.t. } \sum_{n=1}^N \tau[n] \left(\log_2 \left(1 + \frac{1}{S_k[n] I_k^l[n]} \right) - \frac{(\log_2 e)(I_k[n] - I_k^l[n])}{I_k^l[n] + S_k[n] I_k^l[n]^2} \right) \geq \eta^N, \forall k, \quad (56b)$$

$$(16h), (42e), (49b), (51). \quad (56c)$$

Problem (P2.9) now is a convex problem that can be solved efficiently by standard convex program solvers such as CVX [40]. Specifically, we develop an iterative algorithm to optimize the decoding order with given UAV trajectory, time allocation and transmit power as summarized in **Algorithm 2**. Since the application of lower bounds approximation, the obtained result serves a lower bound of that of Problem (P2.8).

Algorithm 2 Penalty-based Algorithm for Decoding Order Design

Initialize the penalty factor λ and feasible solutions $\{\alpha_{k,m}^l[n]\}$ to (P2.8) with given $\{\mathbf{u}[n], T[n], \tau[n], p_k[n]\}$, $l = 0$.

- 1: **repeat**
- 2: Solve Problem (P2.9) with $\{\alpha_{k,m}^l[n]\}$, and denote optimal solutions as $\{\alpha_{k,m}^{l+1}[n]\}$.
- 3: $l = l + 1$.
- 4: **until** the fractional increase of the objective value is below a threshold $\xi > 0$.

D. Overall Algorithm, Complexity and Convergence

Based on the three subproblems in previous subsections, we propose an efficient iterative algorithm to solve Problem (P2) by invoking AO method. The details of the designed algorithm for the NOMA scheme are summarized in Algorithm 3. The complexity of each subproblems with interior-point method are $\mathcal{O}((4N + 4NK)^{3.5})$, $\mathcal{O}((4N + 5NK)^{3.5})$ and $\mathcal{O}(N_{ite}^2(NK^2 + NK)^{3.5})$, respectively, where N_{ite}^2 is the iteration number of Algorithm 2. Therefore, the total complexity for the NOMA scheme is $\mathcal{O}(N_{ite}^N((8N + 9NK)^{3.5} + N_{ite}^2(NK^2 + NK)^{3.5}))$, where N_{ite}^N is the iteration number of Algorithm 3 for the NOMA scheme. It can be seen that complexity of the NOMA scheme is larger than that of the OMA scheme. The convergency of Algorithm 3 can be shown similarly as that of Algorithm 1. The details are omitted due to page limitations.

Algorithm 3 AO-based Algorithm for Problem (P2)

Initialize feasible solutions to (P1)
 $\{\mathbf{u}^0[n], T^0[n], \tau^0[n], p_k^0[n], \alpha_{k,m}^0[n]\}$. $l = 0$.

- 1: **repeat**
- 2: Solve Problem (P2.3) for given $\{p_k^l[n], a_{k,m}^l[n]\}$, denote the optimal solutions as $\{\mathbf{u}^{l+1}[n], T^{l+0.5}[n], \tau^{l+0.5}[n]\}$.
- 3: Solve Problem (P2.5) for given $\{\mathbf{u}^{l+1}[n], a_{k,m}^l[n]\}$, denote the optimal solutions as $\{p_k^{l+1}[n], T^{l+1}[n], \tau^{l+1}[n]\}$.
- 4: Solve Problem (P2.9) with given $\{\mathbf{u}^{l+1}[n], T^{l+1}[n], \tau^{l+1}[n], p_k^{l+1}[n]\}$ via Algorithm 2. Denote the optimal solutions as $\{\alpha_{k,m}^{l+1}[n]\}$.
- 5: $l = l + 1$.
- 6: **until** the fractional increase of the objective value is below a threshold $\xi > 0$.

Proposition 2. For the UAV-enabled IoT system, the NOMA scheme always achieves no worse max-min throughput performance than that of the OMA scheme.

Proof. For any feasible solutions to Problem (P1) in the OMA scheme, it is easy to verify those solutions are also feasible to Problem (P2) in the NOMA scheme. For example, for any $\tau_k[n]$ and $p_k[n]$ in the OMA scheme, we can always construct a feasible solution to the NOMA scheme by making the k th IoT devices transmit with $p_k[n]$ in $\tau[n]$ and other IoT devices' transmit power are zero (remain in silence). Therefore, the OMA scheme can be treated as a special case of the NOMA scheme. It suggests that any feasible solution for the OMA scheme is also feasible for the NOMA scheme, but the reverse does not hold. As a result, the optimal value achieved by the NOMA scheme is always larger than or equal to that of the OMA scheme. \square

V. NUMERICAL RESULTS

In this section, numerical results are provided to evaluate the performances of our proposed algorithms. In the simulations, we consider a UAV-enabled IoT system with $K = 3$ IoT devices, which are randomly and uniformly distributed in a square area of 500×500 m². The UAV is assumed to fly from the initial location $(0, 0, 100)^T$ m to the final location $(500, 500, 100)^T$ m. The height of the UAV is fixed at $H = 100$ m and the maximum UAV speed is $V_{\max} = 30$ m/s. For the rotary-wing UAV propulsion power consumption model in (4), we set the parameters as follows: $P_0 = 79.86$ W, $P_i = 88.63$ W, $U_{tip} = 120$ m/s, $v_0 = 4.03$ m/s, $d_0 = 0.6$, $\rho = 1.225$ kg/m³, $s = 0.05$, $A = 0.503$ m² [27]. The received SNR at a reference distance of 1 m is $\gamma_0 = 50$ dB. The maximum transmit power of IoT devices is set as $P_{\max} = 0.1$ W. We assume that all IoT devices have identical storage energy, e.g. $E_k = E_s, \forall k$. The algorithm threshold ξ is set as 10^{-2} .

In Fig. 2, we first study the convergence of Algorithm 1 and Algorithm 3 for the OMA and NOMA scenarios with $E_s = 10$ Joule (J). The initial UAV trajectory $\{\mathbf{u}^0[n], T^0[n]\}$ is set as the straight flight from the initial location to the final location with the maximum-range (MR) speed in [27]. For the OMA scheme, the time allocation $\{\tau_k^0[n]\}$ and transmit power $\{p_k^0[n]\}$ are obtained by letting $\tau_k^0[n] = \frac{T^0[n]}{K}$ and $p_k^0[n] = \min\left(P_{\max}, E_s \left/ \sum_{n=1}^N \tau_k^0[n]\right.\right), \forall k, n$. For the NOMA scheme, the time allocation $\{\tau^0[n]\}$ and transmit power $\{p_k^0[n]\}$ are obtained by letting $\tau^0[n] = T^0[n]$ and $p_k^0[n] = \min\left(P_{\max}, E_s \left/ \sum_{n=1}^N \tau^0[n]\right.\right), \forall k, n$. We consider two cases with $E_U = 7$ KJ and $E_U = 20$ KJ. From the figure, it is observed that the max-min achievable throughput of three schemes increase quickly with the number of iterations. When $E_U = 7$ KJ,

the proposed algorithm with three schemes converges in about 10 iterations. When $E_U = 20$ KJ, the proposed algorithm converges more fast with around 25 iterations. Therefore, Fig. 2 validate the effectiveness of our proposed algorithms with different multiple access schemes.

In Fig. 3, we provide the optimized UAV trajectory for different multiple access schemes with $E_s = 10$ J and different E_U . In order to illustrate the variety of the instant UAV speed and IoT devices' transmit power shown in Fig. 4, Fig. 3 also presents the time instant when the UAV is closest to each IoT devices in the NOMA scheme. From these figures, it is first observed from Fig. 3 that the UAV tries to successively fly as close as possible to each IoT devices to in both three schemes even with different E_U . This is expected since the max-min throughput objective function we considered makes the UAV need to collect data from each IoT devices in a fair manner. When the UAV on-board energy is small, e.g. $E_U = 8$ KJ, the obtained UAV

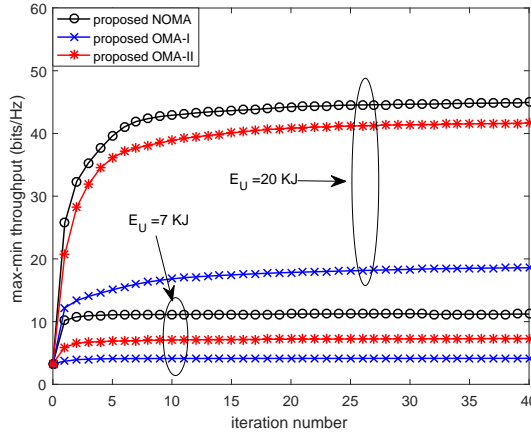


Fig. 2: Convergence of Algorithm 2 with different multiple access schemes.

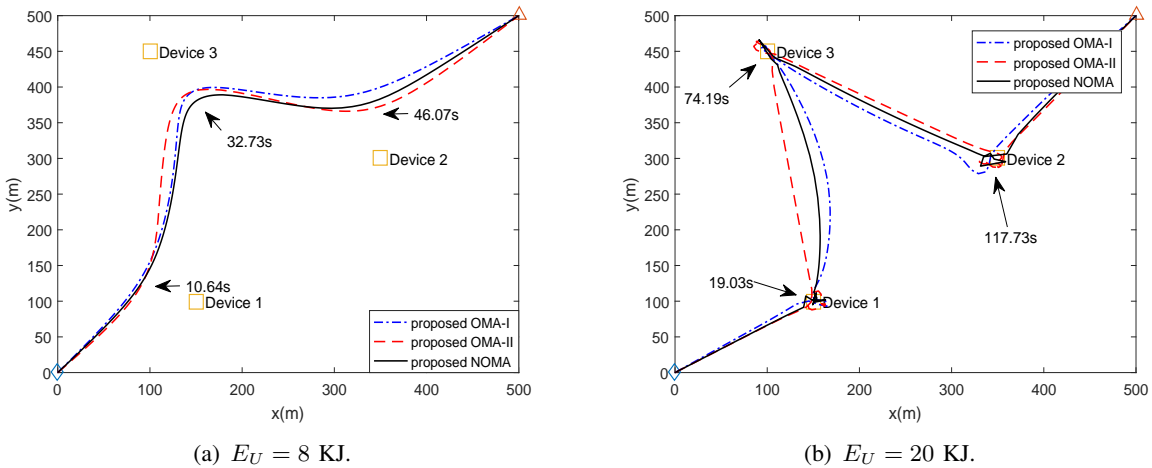


Fig. 3: The optimized UAV trajectories with different multiple access schemes, $E_s = 10$ J.

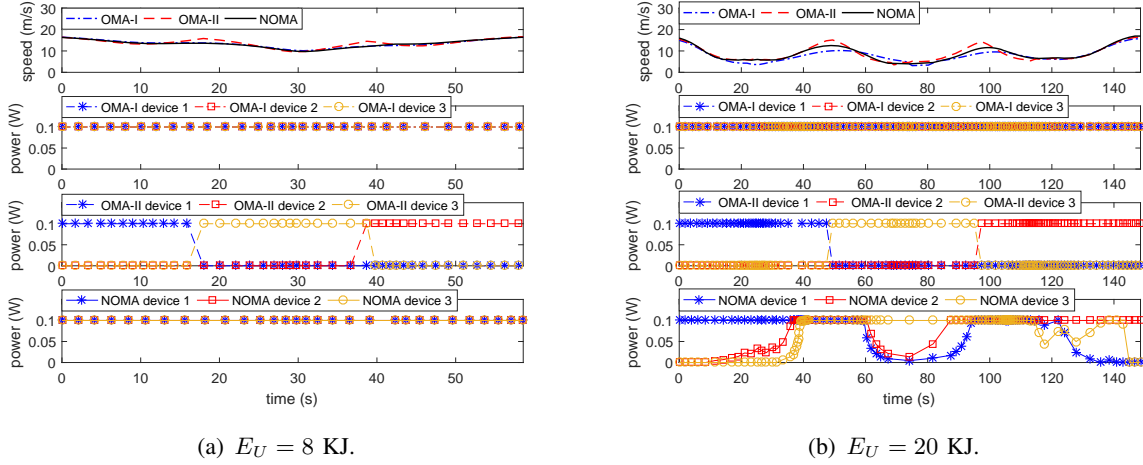


Fig. 4: The optimized UAV speed and transmit power of IoT devices with different multiple access schemes, $E_s = 10$ J.

paths and speeds for three schemes are similar, as shown in Fig. 3(a) and Fig. 4(a). From the perspective of IoT devices' transmit power, the IoT devices transmit at P_{max} when being wakened up by the UAV in all schemes since E_s is large enough compared with the total communication time. For the OMA-II scheme, the IoT devices transmit in a successive manner. This is because the adaptation of time resource allocation in the OMA-II scheme, the UAV only allocates the communication time resource to the nearest IoT device along its trajectory in order to collect more information bits. Though all IoT devices transmit at P_{max} through the whole UAV flight time in the NOMA and OMA-I schemes, the reasons are different. For the NOMA data collection scheme, all devices can multiplex in power level within the same time resource. As a result, the UAV can not only wake up the nearest IoT devices but also other IoT devices to collect more data. However, for the OMA-I scheme, since the time resource is always equally allocated among the IoT devices, the IoT devices need to stay awake to upload more data to the UAV.

In Fig. 3(b) and Fig. 4(b) with $E_U = 20$ KJ, the UAV in general successively flies to the top of each IoT devices in both schemes. It is observed that the UAV keeps flying around at the top of IoT devices other than remaining static. The reason is that the UAV will consume much higher energy to hover in the air than flying around with a certain speed. Thus, the saved energy can prolong the communication time and increase the achieved throughput. Different from the NOMA scheme in Fig. 4(a), there is only one IoT device uploads information sometimes as the manner of the OMA-II scheme when $E_U = 20$ KJ in the NOMA scheme. This is expected since the UAV flight time with $E_U = 20$ KJ is rather large, the storage energy E_s is not enough to let IoT devices keep transmitting. The UAV will wake up the IoT devices as the OMA-II scheme

to get full use of the limited energy stored in each IoT devices. For the OMA-I scheme with $E_U = 20$ KJ, the IoT devices still keep awake during the UAV flight time due to the equal time allocation. It also causes the obtained pathed for the NOMA and OMA-I schemes in Fig. 3(b): the UAV flies a curve between two IoT devices instead of a straight line as the OMA-II scheme since the UAV tends to maximize the rate of all awake IoT devices at the same time.

In Fig. 5, we provide the max-min throughput performance versus the UAV on-board energy E_U with $E_s = 10$ J for different multiple schemes. For comparison, we consider the following benchmark schemes:

- **Straight X:** In this case, the UAV flies from \mathbf{u}_I to \mathbf{u}_F in a straight line. The corresponding max-min achievable throughput is obtained by solving Problem (P1.1) and (P2.1) with additional linear constraints $\mathbf{u}(1, n) = \mathbf{u}(2, n), \forall n$. Meanwhile, X represents different multiple access schemes, such as OMA-I, OMA-II and NOMA.

As illustrated, it is first observed that our proposed optimization schemes significantly outperform those schemes with the straight line UAV trajectory. The performance of our proposed schemes improve with the increase of E_U since the UAV is able to collect more information bits from IoT devices with a longer flight time, which is consistent with **Lemma 1**. Specifically, the NOMA scheme achieves a better performance than those of the two OMA schemes. The performance gain achieved by the NOMA scheme comes from the multiplex of all IoT devices in power domain and the using of SIC technology with additional complexity. The OMA-I scheme has the worst performance. This is expected since the UAV in the OMA-I scheme needs to allocate time resource equally to all IoT devices, which decrease the IoT device's throughput which has

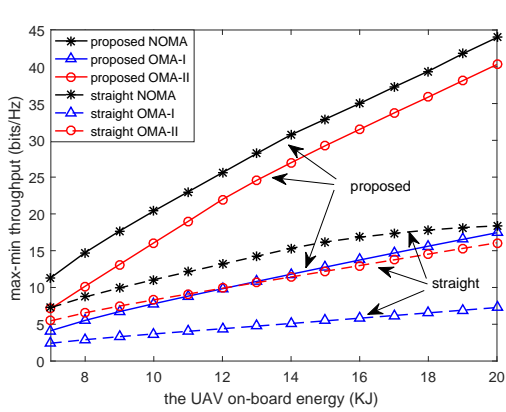


Fig. 5: Max-min throughput versus the UAV onboard energy with $E_s = 10$ J.

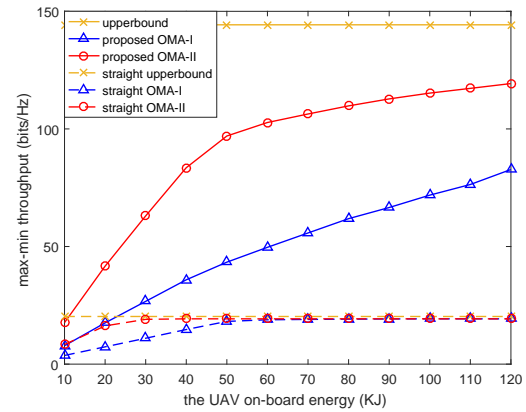


Fig. 6: Max-min throughput versus the UAV on-board energy with $E_s = 10$ J in OMA schemes.

a good channel condition (near from the UAV). It is also observed that the NOMA scheme with straight line UAV trajectory outperforms the OMA-I scheme.

In Fig. 6, we study the analyzed performance upper bound in the OMA schemes. We consider the following two scenarios:

- **Upper bound:** In this scenario, the UAV energy is not considered. The max-min achievable throughput is obtained by solving Problem (P3) with Lemma 1.
- **Straight Upper bound:** This is a special case for the “Upper Bound” scenario, where the UAV flies from \mathbf{u}_I to \mathbf{u}_F in a straight line without the UAV energy constraint.

As illustrated, the max-min throughput performances of the two OMA schemes approach the upper bound as E_U increases in the both scenarios. The OMA-II scheme outperforms the OMA-I scheme due to the adaptive resource allocation. Moreover, the performance gap between the two OMA schemes becomes more narrower as the UAV on-board energy increases.

Finally, Fig. 7 presents the max-min throughput performance versus the device storage energy E_s for different schemes with $E_U = 20$ KJ. From the figure, the performance of all schemes improve with the increase of E_s at first and remain unchanged. This is because for given E_U , the UAV can allocate more time to IoT devices to upload information when E_s increases from a small value. The performances remain unchanged until all the UAV flight time is used for IoT devices uploading data with P_{\max} . In this case, the increase of E_s have no effect on max-min throughput performance since the total energy consumption of IoT devices is fixed. It is also shown that the NOMA scheme always achieves equal or higher max-min throughput than the OMA-II scheme, which is consistent with **Proposition 2**.

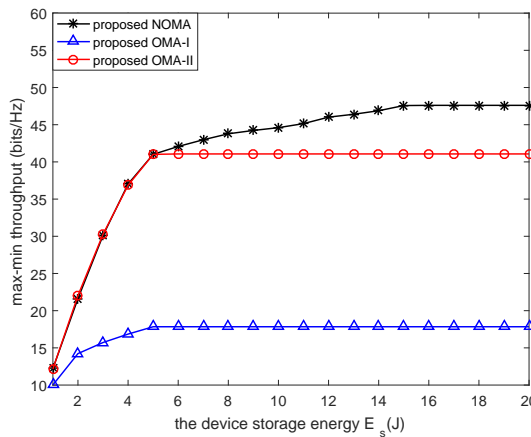


Fig. 7: Max-min throughput versus the IoT device storage energy with $E_U = 20$ KJ.

VI. CONCLUSION

In this paper, the UAV-enabled IoT system has been investigated with various multiple access schemes. The minimum data collection throughput maximization problems were formulated for both OMA and NOMA schemes. To tackle the non-convex problems, two efficient AO-based algorithms were proposed. For the OMA scheme, the original problem was decomposed into two subproblems, which were solved by applying SCA technique. For the NOMA scheme, a penalty-based algorithm was proposed to solve the decoding order design subproblem, while other subproblems were solved with SCA technique. Numerical results verified the effectiveness of our proposed designs compared with other benchmark schemes and demonstrated that the max-min throughput performance obtained with the NOMA scheme is always larger than or equal to the OMA scheme.

APPENDIX A: PROOF OF THEOREM 1

First, the partial Lagrange function of Problem (P2.7) can be expressed as

$$\mathcal{L}(\eta^N, \mathbf{A}, \mathbf{I}, \lambda) = \eta^N + \lambda \left(\sum_{k=1}^K \sum_{m \neq k}^K (\alpha_{k,m}[n]^2 - \alpha_{k,m}[n]) \right), \quad (57)$$

where $\mathbf{A} = \{\alpha_{k,m}[n], k \neq m \in \mathcal{K}, n \in \mathcal{N}\}$, $\mathbf{I} = \{I_k[n], k \in \mathcal{K}, n \in \mathcal{N}\}$ and λ is the non-negative Lagrange multiplier associated with the constraint (50). Therefore, the dual problem of Problem (P2.7) is

$$\min_{\lambda \geq 0} \max_{(\eta^N, \mathbf{A}, \mathbf{I}) \in \mathcal{D}} \mathcal{L}(\eta^N, \mathbf{A}, \mathbf{I}, \lambda) = \min_{\lambda \geq 0} \psi(\lambda), \quad (58)$$

where \mathcal{D} is the feasible set spanned by constraints (16h), (42e), (49b) and (51) and $\psi(\lambda) = \max_{(\eta^N, \mathbf{A}, \mathbf{I}) \in \mathcal{D}} \mathcal{L}(\eta^N, \mathbf{A}, \mathbf{I}, \lambda)$.

Moreover, the primal optimization problem (P2.7) can be equivalently expressed as

$$p^* = \max_{(\eta^N, \mathbf{A}, \mathbf{I}) \in \mathcal{D}} \min_{\lambda \geq 0} \mathcal{L}(\eta^N, \mathbf{A}, \mathbf{I}, \lambda). \quad (59)$$

Due to the weak duality [39], we have the following inequalities:

$$\begin{aligned} \min_{\lambda \geq 0} \psi(\lambda) &= \min_{\lambda \geq 0} \max_{(\eta^N, \mathbf{A}, \mathbf{I}) \in \mathcal{D}} \mathcal{L}(\eta^N, \mathbf{A}, \mathbf{I}, \lambda) \\ &\geq \max_{(\eta^N, \mathbf{A}, \mathbf{I}) \in \mathcal{D}} \min_{\lambda \geq 0} \mathcal{L}(\eta^N, \mathbf{A}, \mathbf{I}, \lambda) = p^*. \end{aligned} \quad (60)$$

It is noted that $\sum_{k=1}^K \sum_{m \neq k}^K (\alpha_{k,m}[n]^2 - \alpha_{k,m}[n]) \leq 0$ for any $\mathbf{A} \in \mathcal{D}$. Thus, $\mathcal{L}(\eta^N, \mathbf{A}, \mathbf{I}, \lambda)$ is a decreasing function with respect to λ for $(\eta^N, \mathbf{A}, \mathbf{I}) \in \mathcal{D}$, which means $\psi(\lambda)$ is bounded from below by the optimal value of Problem (P1.7). Assume that the optimal solutions to the dual problem (58) are λ^* and $(\eta^{N*}, \mathbf{A}^*, \mathbf{I}^*)$. In the following, we discuss the optimal value of the

dual problem (58) and the equivalent primal problem (59) in two cases.

First, suppose that $\sum_{k=1}^K \sum_{m \neq k}^K (\alpha_{k,m}^*[n]^2 - \alpha_{k,m}^*[n]) = 0$. Since $(\eta^{N*}, \mathbf{A}^*, \mathbf{I}^*)$ are also feasible to Problem (59), we have the following inequalities:

$$p^* \geq \eta^{N*} = \mathcal{L}(\eta^{N*}, \mathbf{A}^*, \mathbf{I}^*, \lambda^*) = \psi(\lambda^*). \quad (61)$$

Based on (60) and (60), we have

$$\begin{aligned} \max_{(\eta^N, \mathbf{A}, \mathbf{I}) \in \mathcal{D}} \min_{\lambda \geq 0} \mathcal{L}(\eta^N, \mathbf{A}, \mathbf{I}, \lambda) \\ = \min_{\lambda \geq 0} \max_{(\eta^N, \mathbf{A}, \mathbf{I}) \in \mathcal{D}} \mathcal{L}(\eta^N, \mathbf{A}, \mathbf{I}, \lambda), \end{aligned} \quad (62)$$

which implies the strong duality between the equivalent primal problem (59) and the dual problem (58) holds when $\sum_{k=1}^K \sum_{m \neq k}^K (\alpha_{k,m}^*[n]^2 - \alpha_{k,m}^*[n]) = 0$. Recall from that $\mathcal{L}(\eta^N, \mathbf{A}, \mathbf{I}, \lambda)$ is a decreasing function with respect to λ , we have

$$\psi(\lambda) = p^*, \forall \lambda \geq \lambda^*. \quad (63)$$

Second, when $\sum_{k=1}^K \sum_{m \neq k}^K (\alpha_{k,m}^*[n]^2 - \alpha_{k,m}^*[n]) < 0$, $\psi(\lambda^*) = \min_{\lambda \geq 0} \psi(\lambda) \rightarrow -\infty$ due to the monotone decreasing of $\psi(\lambda)$ with respect to λ . This contradicts the inequality in (60) since p^* is a finite value.

Above all, $\sum_{k=1}^K \sum_{m \neq k}^K (\alpha_{k,m}^*[n]^2 - \alpha_{k,m}^*[n]) = 0$ must hold at the optimal solution and the proof of Theorem 1 is completed.

REFERENCES

- [1] A. Zanella, N. Bui, A. Castellani, L. Vangelista, and M. Zorzi, “Internet of Things for smart cities,” *IEEE Internet Things J.*, vol. 1, no. 1, pp. 22–32, Feb 2014.
- [2] A. Al-Fuqaha, M. Guizani, M. Mohammadi, M. Aledhari, and M. Ayyash, “Internet of Things: A survey on enabling technologies, protocols, and applications,” *IEEE Commun. Surv. Tut.*, vol. 17, no. 4, pp. 2347–2376, Fourthquarter 2015.
- [3] J. Lin, W. Yu, N. Zhang, X. Yang, H. Zhang, and W. Zhao, “A survey on Internet of Things: Architecture, enabling technologies, security and privacy, and applications,” *IEEE Internet Things J.*, vol. 4, no. 5, pp. 1125–1142, Oct 2017.
- [4] K. Chi, Z. Chen, K. Zheng, Y. Zhu, and J. Liu, “Energy provision minimization in wireless powered communication networks with network throughput demand: TDMA or NOMA?” *IEEE Trans. Commun.*, vol. 67, no. 9, pp. 6401–6414, Sep. 2019.
- [5] M. Shirvanimoghaddam, M. Dohler, and S. J. Johnson, “Massive non-orthogonal multiple access for cellular IoT: Potentials and limitations,” *IEEE Commun. Mag.*, vol. 55, no. 9, pp. 55–61, Sep. 2017.
- [6] N. H. Motlagh, M. Bagaa, and T. Taleb, “UAV-based IoT platform: A crowd surveillance use case,” *IEEE Commun. Mag.*, vol. 55, no. 2, pp. 128–134, February 2017.
- [7] A. Al-Hourani, S. Kandeepan, and A. Jamalipour, “Modeling air-to-ground path loss for low altitude platforms in urban environments,” in *Proc. IEEE Global Commun. Conf. (GLOBECOM)*, Dec 2014, pp. 2898–2904.
- [8] Y. Liu, Z. Qin, M. Elkashlan, Z. Ding, A. Nallanathan, and L. Hanzo, “Nonorthogonal multiple access for 5G and beyond,” *Proc. IEEE*, vol. 105, no. 12, pp. 2347–2381, Dec 2017.

- [9] Y. Cai, Z. Qin, F. Cui, G. Y. Li, and J. A. McCann, “Modulation and multiple access for 5G networks,” *IEEE Commun. Surv. Tut.*, vol. 20, no. 1, pp. 629–646, Firstquarter 2018.
- [10] Z. Chen, Z. Ding, X. Dai, and R. Zhang, “An optimization perspective of the superiority of NOMA compared to conventional OMA,” *IEEE Trans. Signal Process.*, vol. 65, no. 19, pp. 5191–5202, Oct 2017.
- [11] Z. Ding, Z. Yang, P. Fan, and H. V. Poor, “On the performance of non-orthogonal multiple access in 5G systems with randomly deployed users,” *IEEE Signal Process. Lett.*, vol. 21, no. 12, pp. 1501–1505, Dec 2014.
- [12] Z. Yang, Z. Ding, P. Fan, and N. Al-Dhahir, “A general power allocation scheme to guarantee quality of service in downlink and uplink NOMA systems,” *IEEE Trans. Wireless Commun.*, vol. 15, no. 11, pp. 7244–7257, Nov 2016.
- [13] J. Choi, “Power allocation for max-sum rate and max-min rate proportional fairness in NOMA,” *IEEE Wireless Commun. Lett.*, vol. 20, no. 10, pp. 2055–2058, Oct 2016.
- [14] Y. Liu, Z. Ding, M. Elkashlan, and H. V. Poor, “Cooperative non-orthogonal multiple access with simultaneous wireless information and power transfer,” *IEEE J. Sel. Areas Commun.*, vol. 34, no. 4, pp. 938–953, April 2016.
- [15] M. S. Ali, E. Hossain, A. Al-Dweik, and D. I. Kim, “Downlink power allocation for CoMP-NOMA in multi-cell networks,” *IEEE Trans. Commun.*, vol. 66, no. 9, pp. 3982–3998, Sep. 2018.
- [16] Y. Liu, Z. Qin, M. Elkashlan, Y. Gao, and L. Hanzo, “Enhancing the physical layer security of non-orthogonal multiple access in large-scale networks,” *IEEE Trans. Wireless Commun.*, vol. 16, no. 3, pp. 1656–1672, March 2017.
- [17] D. Zhai, R. Zhang, L. Cai, B. Li, and Y. Jiang, “Energy-efficient user scheduling and power allocation for NOMA-based wireless networks with massive IoT devices,” *IEEE Internet Things J.*, vol. 5, no. 3, pp. 1857–1868, June 2018.
- [18] T. Lv, Y. Ma, J. Zeng, and P. T. Mathiopoulos, “Millimeter-wave NOMA transmission in cellular M2M communications for Internet of Things,” *IEEE Internet Things J.*, vol. 5, no. 3, pp. 1989–2000, June 2018.
- [19] Q. Wu, W. Chen, D. W. K. Ng, and R. Schober, “Spectral and energy-efficient wireless powered iot networks: NOMA or TDMA?” *IEEE Trans. Veh. Technol.*, vol. 67, no. 7, pp. 6663–6667, July 2018.
- [20] A. Al-Hourani, S. Kandeepan, and S. Lardner, “Optimal LAP altitude for maximum coverage,” *IEEE Wireless Commun. Lett.*, vol. 3, no. 6, pp. 569–572, Dec 2014.
- [21] M. Mozaffari, W. Saad, M. Bennis, and M. Debbah, “Efficient deployment of multiple unmanned aerial vehicles for optimal wireless coverage,” *IEEE Wireless Commun. Lett.*, vol. 20, no. 8, pp. 1647–1650, Aug 2016.
- [22] J. Lyu, Y. Zeng, R. Zhang, and T. J. Lim, “Placement optimization of UAV-mounted mobile base stations,” *IEEE Wireless Commun. Lett.*, vol. 21, no. 3, pp. 604–607, March 2017.
- [23] M. Mozaffari, W. Saad, M. Bennis, and M. Debbah, “Unmanned aerial vehicle with underlaid device-to-device communications: Performance and tradeoffs,” *IEEE Trans. Wireless Commun.*, vol. 15, no. 6, pp. 3949–3963, 2016.
- [24] Q. Wu, Y. Zeng, and R. Zhang, “Joint trajectory and communication design for multi-UAV enabled wireless networks,” *IEEE Trans. Wireless Commun.*, vol. 17, no. 3, pp. 2109–2121, March 2018.
- [25] Y. Cai, F. Cui, Q. Shi, M. Zhao, and G. Y. Li, “Dual-UAV-enabled secure communications: Joint trajectory design and user scheduling,” *IEEE J. Sel. Areas Commun.*, vol. 36, no. 9, pp. 1972–1985, Sep. 2018.
- [26] C. You and R. Zhang, “3D trajectory optimization in rician fading for UAV-enabled data harvesting,” *IEEE Trans. Wireless Commun.*, vol. 18, no. 6, pp. 3192–3207, June 2019.
- [27] Y. Zeng, J. Xu, and R. Zhang, “Energy minimization for wireless communication with rotary-wing UAV,” *IEEE Trans. Wireless Commun.*, vol. 18, no. 4, pp. 2329–2345, April 2019.
- [28] J. Gong, T. Chang, C. Shen, and X. Chen, “Flight time minimization of UAV for data collection over wireless sensor networks,” *IEEE J. Sel. Areas Commun.*, vol. 36, no. 9, pp. 1942–1954, Sep. 2018.
- [29] C. Zhan and H. Lai, “Energy minimization in Internet-of-Things system based on rotary-wing UAV,” *IEEE Wireless Commun. Lett.*, pp. 1–1, 2019.

- [30] Y. Sun, D. Xu, D. W. K. Ng, L. Dai, and R. Schober, "Optimal 3D-trajectory design and resource allocation for solar-powered UAV communication systems," *IEEE Trans. Commun.*, vol. 67, no. 6, pp. 4281–4298, June 2019.
- [31] Y. Liu, Z. Qin, Y. Cai, Y. Gao, G. Y. Li, and A. Nallanathan, "UAV communications based on non-orthogonal multiple access," *IEEE Wireless Commun.*, vol. 26, no. 1, pp. 52–57, February 2019.
- [32] M. F. Sohail, C. Y. Leow, and S. Won, "Non-orthogonal multiple access for unmanned aerial vehicle assisted communication," *IEEE Access*, vol. 6, pp. 22 716–22 727, 2018.
- [33] T. Hou, Y. Liu, Z. Song, X. Sun, and Y. Chen, "Multiple antenna aided NOMA in UAV networks: A stochastic geometry approach," *IEEE Trans. Commun.*, vol. 67, no. 2, pp. 1031–1044, Feb 2019.
- [34] W. Mei and R. Zhang, "Uplink cooperative NOMA for cellular-connected UAV," *IEEE J. Sel. Topics Signal Process.*, vol. 13, no. 3, pp. 644–656, June 2019.
- [35] R. Duan, J. Wang, C. Jiang, H. Yao, Y. Ren, and Y. Qian, "Resource allocation for multi-UAV aided IoT NOMA uplink transmission systems," *IEEE Internet Things J.*, vol. 6, no. 4, p. 7025C7037, Aug 2019.
- [36] F. Cui, Y. Cai, Z. Qin, M. Zhao, and G. Y. Li, "Multiple access for mobile-UAV enabled networks: Joint trajectory design and resource allocation," *IEEE Trans. Commun.*, vol. 67, no. 7, p. 4980C4994, July 2019.
- [37] N. Zhao, X. Pang, Z. Li, Y. Chen, F. Li, Z. Ding, and M. Alouini, "Joint trajectory and precoding optimization for UAV-assisted NOMA networks," *IEEE Trans. Commun.*, vol. 67, no. 5, pp. 3723–3735, May 2019.
- [38] 3GPP-TR-36.777, "Study on enhanced LTE support for aerial vehicles," 2017, 3GPP technical report.[Online]. Available:www.3gpp.org/dynareport/36777.htm.
- [39] S. Boyd and L. Vandenberghe, *Convex Optimization*. Cambridge, U.K.: Cambridge Univ. Press, 2004.
- [40] M. Grant and S. Boyd, "CVX: Matlab software for disciplined convex programming, version 2.1," [Online]. Available:<http://cvxr.com/cvx>, Mar 2014.